SRTTU
Journal of Computational and Applied Research in Mechanical Engineering
jcarme.sru.ac.ir
JCARME
ISSN: 2228-7922

Research paper

A novel 1D model approach to optimize the entrainment ratio of a steam ejector and introducing novel definitions of ejector efficiency

S. Akbarnejad and M. Ziabasharhagh*

Dept. of Mech. Eng., K. N. Toosi University of Technology., Tehran, Iran

Article info:

Article history:

Received: 00/00/0000
Accepted: 00/00/0018
Revised: 00/00/0000
Online: 00/00/0000

Keywords:
Supersonic,
Ejector,
CFD,
Geometry,
Efficiency.

***Corresponding author:**
mzia@kntu.ac.ir

Abstract

This paper presents a novel 1D modeling approach to optimize steam ejector entrainment ratios, introducing new definitions of ejector efficiency and methods for enhancement. Using the proposed model, an ejector is tailored for specific boundary conditions with available CFD results for validation. Dimensional and geometrical parameters are computed from the theoretical 1D model, and various geometries are explored using CFD to determine entrainment ratios.

Innovative definitions of ejector efficiency are introduced. The first definition compares the entrainment ratio of the ejector to a system comprising a steam compressor, turbine, and mixer, yielding an efficiency of 13.5% under specified conditions. The second, more practical definition calculates the maximum achievable entrainment ratio, disregarding frictional losses, resulting in an efficiency of 70%.

An algorithm is proposed to optimize ejector dimensions to approach this maximum. Using this algorithm, the optimum throat diameter was determined through CFD analysis, demonstrating an increase in the entrainment ratio from 0.7 to 1.25. The theoretical maximum value calculated by the 1D model is 1.282, indicating 97.7% of the theoretical maximum was achieved in CFD simulations. This highlights the significant improvement in the entrainment ratio using the 1D model and delineates its limit under given conditions.

The third definition establishes the theoretical maximum entrainment ratio given specific boundary conditions and dimensions, assuming no losses in the nozzle, mixing process, or diffuser, yielding an efficiency of 81% for the same ejector studied.

1. Introduction

Ejectors find extensive use in refrigeration systems [1–5], particularly in solar-driven ejector refrigeration systems [6] and [7]. Other applications include thrust augmentation [8], high altitude simulation (HAT) facility [9], solid material conveying, waste heat recovery and vacuum desalination systems, among others.

In comparison to mechanical compressors, ejectors offer several advantages due to their lack of moving parts. However, ejectors

generally exhibit significantly lower efficiencies when compared to mechanical compressors[10].

Various investigations have been conducted to enhance the efficiency of ejectors, which can be broadly categorized into two groups:

1. Optimization of the nozzle and ejector geometry through experimental and computational fluid dynamics techniques [11–13].
2. Studying the effect of boundary conditions and working fluid properties on ejector performance [14], [15].

Numerous attempts have been made to enhance the ejector efficiency through geometrical optimization. The impact of nozzle exit position (NXP) on the ejector performance has been explored by various researchers [16–21]. In addition, certain studies have concentrated on variable area ejectors [22–24].

Area Ratio (Ar), which denotes the ratio between the constant area section and primary nozzle throat areas, is another crucial factor that significantly influences the ejector's performance. For instance, Hakkaki Fard et al. [25] discovered that increasing the area ratio results in the shifting of shock waves away from the constant area section. Other researchers have found an optimal value for the diameter ratio [26], [27].

Further investigations have been undertaken on the mixing section of the ejector. Jeong et al.[28] studied the converging angle of the mixing section, whereas Krzysztof Banasiak et al. [29] found that reducing the mixing section diameter leads to a small reduction in the ejector's irreversibility. Stefan Elbel and Pega Hrnjak [30] determined the optimal diffuser angle for a prototype ejector.

While various factors, such as entrainment ratio and pressure ratio, have been used to assess the efficiency of ejectors, no ideal efficiency has been established as a reference for comparing the actual efficiency of ejectors with that of an ideal one. The Carnot cycle efficiency serves as an example of the maximum attainable efficiency for a heat engine operating between specified temperature limits. Several studies have been conducted to enhance the entrainment ratio of a steam ejector while maintaining the same pressure at the evaporator, condenser, and boiler, by altering the geometry of the ejector or nozzle. A few researchers have succeeded in increasing the entrainment ratio by a small percentage. However, The highest attainable entrainment ratio for an ideal steam ejector in optimal geometry and without losses is still unknown. Additionally, it is challenging to determine whether an ejector design with a specified entrainment ratio is effective or not, and to what extent the entrainment ratio can be increased.

To address these issues, we propose three different efficiencies. The first efficiency compares the performance of an ejector system with that of a system consisting of a steam compressor, a steam turbine, and a mixer used to mix two streams.

Efficiency 2 is defined as the maximum entrainment ratio achievable by an ejector with a specific geometry, assuming an ideal efficiency of 1 for the nozzle, mixing process, and diffuser, while disregarding friction and other losses. To determine the maximum possible entrainment ratio, a 1D model is employed. On the other hand, Efficiency 3 is defined as the maximum entrainment ratio that can be attained by an ejector with known boundary conditions, by choosing the appropriate size and geometry. This efficiency is obtained by dividing the entrainment ratio of the specified ejector by the theoretical maximum entrainment ratio computed from the 1D model under the same boundary conditions. To demonstrate these efficiencies, we will examine an ejector from prior studies and show how the newly developed 1D model can increase the entrainment ratio. This process involves conducting CFD simulations of an ejector studied by Ariafar [31], aiming to attain the maximum theoretically possible entrainment ratio within specified boundary conditions. Initially, our CFD approach is validated by comparing the entrainment ratio and static pressure results along the ejector with those reported in Al_Doori's work [10]. Utilizing the same approach and settings, various parameters are adjusted, and multiple CFD simulations are carried out to achieve the maximum theoretical entrainment ratio of the ejector studied by Ariafar [31], maintaining the same boundary

conditions but with optimized calculated ejector throat diameter and other geometrical parameters.

2. Ejector operation principle

A schematic picture of the steam jet ejector is shown in Fig. 1.

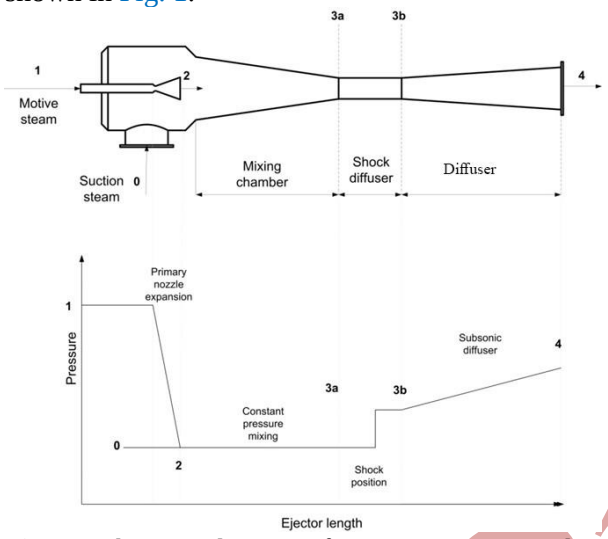

Fig. 1. Schematic diagram of steam jet ejector and pressure variation along its length.

The high-pressure motive vapor at 1 expands to the suction vapor pressure at 0. The high-velocity jet at 2 entrains the suction vapor and mixing occurs at constant pressure. The state after mixing at 3a is still at a very high velocity (supersonic). The mixing chamber is followed by a constant area section, where a normal shock could occur. Upon experiencing the shock at 3b, the fluid stream, consisting of both the motive and suction, is compressed to the condenser pressure to attain state 4 in the diffuser section.

The primary pressure ratio of ejectors is defined as the ratio of steam supply pressure to discharge pressure or:

$$N_p = p_1/p_4 \quad (1)$$

And Compression ratio is defined as the ratio of discharge pressure to secondary inlet pressure or:

$$N_s = p_4/p_0 \quad (2)$$

The main objective of this study is to increase the entrainment ratio which is defined as:

$$ER = \frac{\dot{m}_s}{\dot{m}_p} \quad (3)$$

This parameter is of great importance as by increasing the entrainment ratio, less motive steam is consumed at the same suction mass flow rate.

3. Introduction of novel definitions for an ejector efficiency

3.1 Efficiency #1: ejector compared to a system composed of a steam compressor, a steam turbine, and a mixer to mix two streams

As discussed before, steam ejectors have a wide application in several industries including water desalination plants. These plants employ high-pressure live steam to elevate the pressure and temperature of suction steam for subsequent use in the evaporator's succeeding stages. Despite their reliability, low maintenance requirements, and cost-effectiveness as compared to mechanical compressors, the efficiency of steam ejectors is relatively low. Nevertheless, in plants where low-grade steam is produced as a byproduct or available at low cost, steam jet ejectors are a preferred option over mechanical compressors. For example, in sulfuric acid plants, a substantial amount of high-pressure steam is generated for cooling sulfur dioxide gas. Such steam is typically either vented or condensed to produce deionized water. However, a system composed of a steam compressor, steam turbine, and mixer can be employed to replace steam ejectors, even if excess or free steam is available in certain plants. As illustrated in Fig. 2, a steam turbine can extract the energy of high-pressure steam at point 1 and convert it into work, which can then be transferred to the steam compressor for compressing the suction steam at point 0 to condenser pressure (point 4).

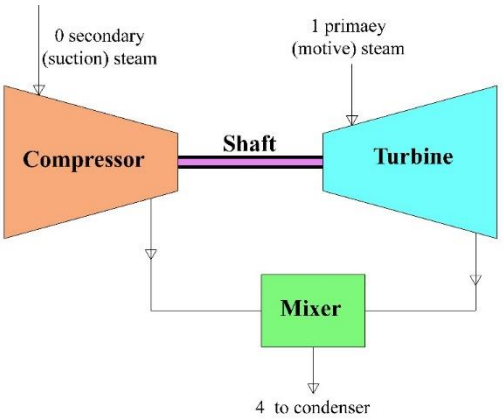

Fig. 2 Modeling an ejector as a combination of a compressor, a turbine, and a mixer.

The amount of work generated in the steam turbine is equal to the amount of work needed to increase the pressure of suction steam to condenser pressure (i.e. the whole work generated in the steam turbine is consumed in the compressor). It is assumed that the pressure at the outlet of the compressor and turbine is the same and is equal to the condenser pressure.

$$W_{comp.} = \dot{m}_p(h_1 - h_{4s}) \quad (4)$$

$$W_{turb.} = \dot{m}_s(h_0 - h_{4s}) \quad (5)$$

Considering the isentropic efficiency of 1 for both compressor and steam turbine (isentropic compression and expansion), if one unit of mass of live steam is available, the maximum amount of suction steam that will be compressed to condenser pressure can be calculated by simplifying Eq. (4) and Eq. (5) as:

$$ER = \frac{h_1 - h_{4s}}{h_0 - h_{4s_{max}}} \quad (6)$$

So, if the pressure and temperature of live steam and suction steam, and discharge pressure are known, the maximum possible entrainment ratio can be calculated by the above formula. Now the efficiency of the ejector is defined as the entrainment ratio of a specified ejector to that of a system composed of a compressor and steam turbine.

$$\eta_1 = \frac{ER}{ER_{max}} \quad (7)$$

To illustrate the application of this efficiency, the steam ejector of Ariafar [31] is used in this paper. Based on the live steam, suction, and discharge pressures of 700, 22.85, and 30 kPa, respectively, the maximum achievable entrainment ratio for a system consisting of a compressor and steam turbine is 6.67. In comparison, the entrainment ratio reported for the ejector operating under the same boundary conditions is 0.9, yielding an efficiency of 13.5%. This efficiency is considerably lower than that of the compressor and steam turbine system.

3.2 Efficiency #2: definition of ejector efficiency based on the 1D model #1

In the previous section, the entrainment ratio of the ejector of Ariafar work [31] to that of a system composed of a compressor and steam turbine was calculated and considered as the first definition of efficiency. However, it would be more convenient to establish the maximum achievable entrainment ratio of an ejector under the same boundary conditions, irrespective of its dimensions and geometry, while disregarding frictional losses. Such an efficiency metric would enable a direct comparison of the ejector's performance with an ideal one under identical boundary conditions without reference to a compressor and steam turbine system.

This section aims to compute the maximum entrainment ratio attainable by an ejector subject to specific boundary conditions. The Ariafar model [31] is employed once again as a benchmark to illustrate the calculation. Assume that the primary steam passes through the converging-diverging primary nozzle with a mass of m_1 kg. As the primary steam expands through the converging-diverging primary nozzle, it reaches the suction pressure, which is consistent with the constant pressure mixing model examined in this study. Neglecting the gas velocity at the inlet of the nozzle, which is a reasonable assumption given the supersonic velocity at the nozzle exit, the velocity of the

primary steam at point 2 can be estimated using the energy equation:

$$C_2 = \sqrt{2(h_1 - h_2)} \quad (8)$$

Note that no loss is considered in the above equation as an ideal entrainment ratio should be calculated.

For the constant pressure mixing zone, an initial value for the mass flow rate of secondary (suction) steam (m_0) is guessed. Using the continuity and momentum equation and with the assumption of constant pressure mixing, the speed of the mixed stream (C_{3a}) can be calculated according to Eq. (9):

$$m_3 C_{3a} = m_1 C_2 \quad (9)$$

Here again, mixing efficiency is considered 100% and no loss is considered in the calculation. The secondary flow speed at its entrance is neglected too.

Having calculated the speed of the mixture at point 3a, using the energy equation, the enthalpy of the mixture can be calculated:

$$m_1 h_1 + m_0 h_0 = m_3 \left(h_{3a} + \frac{{C_{3a}}^2}{2} \right) \quad (10)$$

By knowing the enthalpy of the mixture at point 3a and its pressure which is assumed to be equal to p_0 (the constant pressure mixing model), all other thermodynamic properties of the mixture including its specific volume (v_{3a}) can be extracted from steam tables. Then the constant area section area can be calculated using the continuity equation:

$$m_3 = \frac{C_{3a} A}{v_{3a}} \quad (11)$$

For the constant area section, a normal shock wave is generated to increase the pressure of the flow. For this section, we have 3 equations (continuity, momentum, and energy) available:

$$\frac{C_{3a}}{v_{3a}} = \frac{C_{3b}}{v_{3b}} \quad (12)$$

$$(P_{3b} - P_{3a})A = (C_{3a} - C_{3b})m_3 \quad (13)$$

$$h_{3a} + \frac{{C_{3a}}^2}{2} = h_{3b} + \frac{{C_{3b}}^2}{2} \quad (14)$$

But there are four unknowns (C_{3b}, P_{3b}, h_{3b}, and v_{3b}). So iterative approach is used. An initial value for C_{3b} is guessed and, P_{3b}, h_{3b}, and v_{3b} are calculated from the equations (12)-(15).knowing P_{3b} and v_{3b}, the value of enthalpy h'_{3b} can be extracted from steam tables. If the difference between this enthalpy read from steam tables and the value of enthalpy calculated from the energy equation is less than a defined small value ε, then the iteration is ended otherwise a new value for C_{3b} is guessed.

$$h'_{3b} - h_{3b} < |\varepsilon| \quad (15)$$

For the diffuser section, considering the isentropic expansion of steam and negligible speed of the flow at the exit of the diffuser, the enthalpy at exit is calculated using the energy equation:

$$h_4 - h_{3a} = \frac{{C_{3b}}^2}{2} \quad (16)$$

And with the assumption of isentropic expansion, we know the entropy of the mixture at point 4 is $s_4 = s_{3b}$. By knowing s_4 and h_4, the pressure at point 4 (P_4)can be extracted from steam tables. If P_4 it is below the designed discharge pressure, the guessed value m_0 should be decreased by Δm_0 and the iteration process should continue until the difference between P_4 and the design outlet pressure is less than a defined small value. The iterative procedure flowchart is described in Fig. 3:

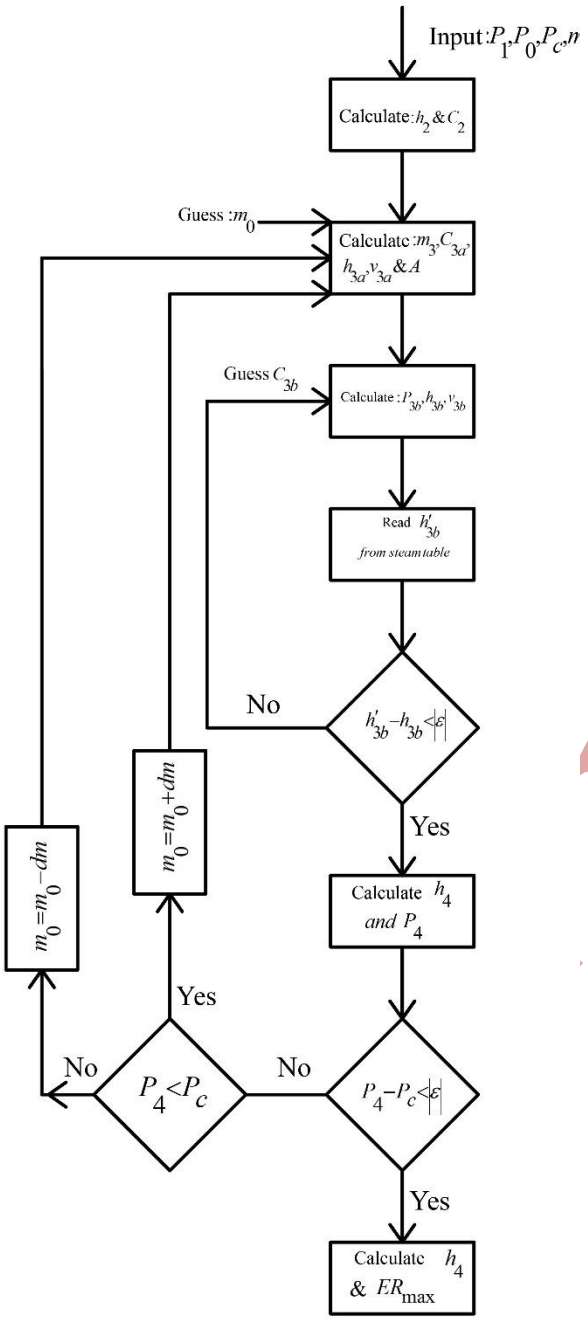

Fig. 3. The iterative procedure flowchart for maximizing the entrainment ratio of an ejector.

Considering live steam, suction, and discharge pressure of 700, 22.85, and 35 kPa respectively, the maximum entrainment ratio of an ejector based on the above-mentioned 1D iterative model is calculated 1.282 while the entrainment ratio of the ejector of Ariafar work [31] with the same boundary condition calculated by CFD simulation is reported 0.9. So, a second efficiency can be defined as the following:

$$\eta_2 = \frac{ER}{ER_{max-1D\,model}} \qquad (17)$$

This efficiency for the Ariafar ejector [31] is

$$\eta_2 = \frac{0.9}{1.282} = 70\%$$

3.3 Efficiency #3: ideal efficiency of an ejector with a given geometry (1D model #2)

Here, it is assumed that the diameter of the primary nozzle throat and the ejector's throat (constant area section) are known. The aim is to compare the entrainment ratio of an ejector calculated by CFD simulations or experiments to that of an ideal 1D theoretical model. This efficiency is useful in predicting how much the entrainment ratio of the ejector can be enhanced if there was no friction and losses associated with vortexes, heat transfer from the body of the ejector, and other sources of irreversibilities. This efficiency shows how far the entrainment ratio of an ejector can be increased by decreasing or eliminating losses and frictions (for example by decreasing the surface roughness of the nozzle and ejector). In this definition of efficiency, changing the diameter of the primary nozzle throat and the ejector's throat is not allowable. However, the primary nozzle exit diameter and position can be adjusted to increase the ejector's performance.

This section considers a scenario in which the diameters of the primary nozzle throat and the constant area section of the ejector throat are predetermined. The objective is to contrast the entrainment ratio of an ejector determined through computational fluid dynamics (CFD) simulations or experiments with that of an ideal one-dimensional (1D) theoretical model. This efficiency metric is beneficial in projecting the degree to which the ejector's entrainment ratio could be amplified in the absence of friction, vortex losses, heat transfer from the ejector body, and other sources of irreversibility. It provides insight into how much the ejector's entrainment ratio can be elevated by reducing or eliminating losses and frictions (for example, by

minimizing the surface roughness of the nozzle and ejector). Altering the diameters of the primary nozzle throat and the ejector's throat is not permitted in this efficiency definition. However, the position and exit diameter of the primary nozzle can be adjusted to increase the ejector's performance.

Fig. 4 depicts the flowchart for computing the maximum entrainment ratio using an ideal 1D theoretical model. Assuming the diameters of the primary nozzle throat and the ejector's throat are known (i.e. d_{th} and d_3), the mass flow rate through the primary nozzle can be calculated using ideal gas relations for choked flow. Given the thermodynamic properties of the steam at point 1, the mass flow rate of primary steam can be computed using Eq. (18):

$$m_1 = A_{th}\sqrt{\gamma\rho_1 P_1\left(\frac{2}{\gamma+1}\right)^{\frac{\gamma+1}{\gamma-1}}} \qquad (18)$$

In the next step, an initial value of the mass flow rate of secondary steam is guessed. The value of mixed steam at point 3a (C_{3a}) is calculated by using Eq. (10).

Then the area at the throat of the ejector (A_3') is calculated by Eq. (11).

If the difference between the calculated value of the area at the throat of the ejector (A_3')and the given value of the diameter of the ejector's throat is less than a specified value ε, the iteration is terminated and pressure at points 3b and 4 are calculated using the iterative method for calculation of pressure after the normal shock wave which was described in the previous section. Otherwise, if the calculated value of the area at the throat of the ejector (A_3') is greater than the given value of the diameter of the ejector's throat, then the guess value for the secondary steam mass flow rate should be lowered by a small amount of dm otherwise it should be increased by dm.

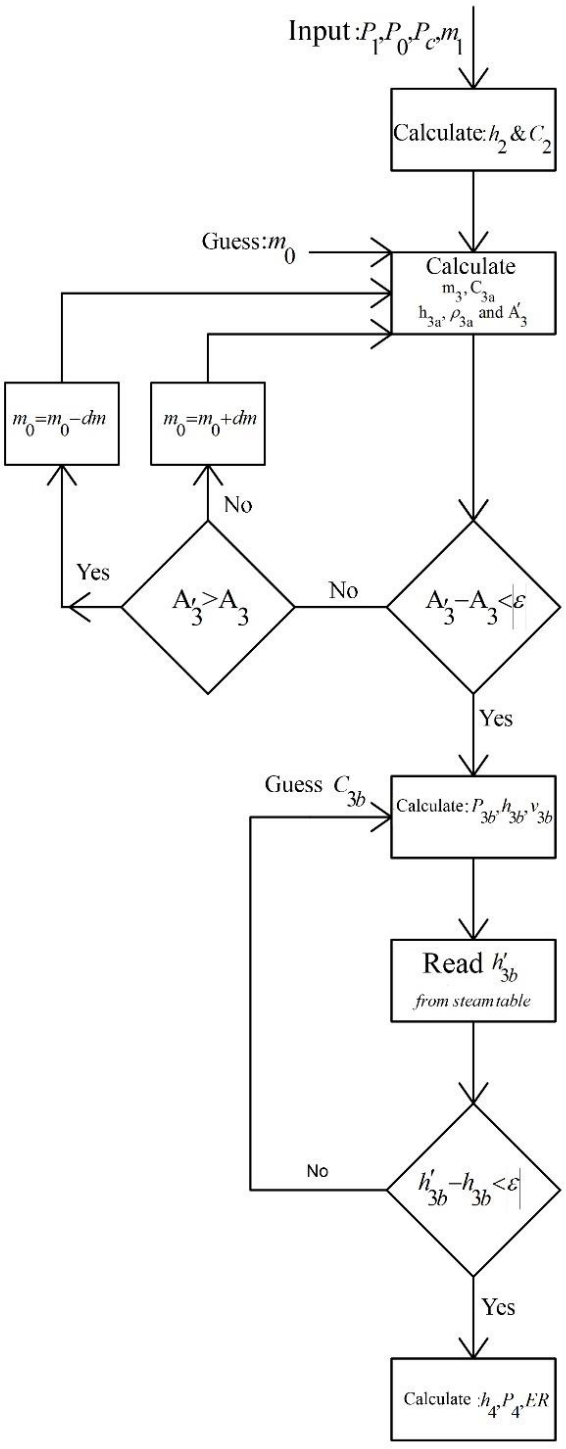

Fig. 4. Flowchart for calculating the ideal efficiency of an ejector (η_3).

The Ariafar ejector utilized in previous research [31] has been selected once again, using the same boundary conditions consisting of live

steam, suction, and discharge pressure set at 700, 22.85, and 35 kPa respectively. The diameters of the primary nozzle throat and ejector throat remain unchanged at 26 mm and 140 mm, respectively. The ejector's ideal efficiency was calculated using the procedure outlined in Fig. 4 , resulting in a value of 1.11. Comparatively, the entrainment ratio of the Ariafar ejector under the same boundary conditions was determined to be 0.9 through CFD simulation. As a result, a third efficiency can be defined as:

$$\eta_3 = \frac{ER}{ER_{\max-1D-\mathrm{mod}el2}} \quad (19)$$

This efficiency for the Ariafar ejector [31] is $\eta_3 = \frac{0.9}{1.11} = 81\%$. It means that this ejector with the specified boundary conditions and fixed primary nozzle throat and the ejector's throat diameter can reach a maximum entrainment ratio of 1.11 if no losses occur in the ejector.

4. Enhancing ejector efficiency via the 1D iterative model and computational fluid dynamics (CFD) simulations

In the preceding section, it was demonstrated that for an ejector with a constant pressure mixing design, subject to boundary conditions of live steam, suction, and discharge pressures of 700, 22.85, and 40 kPa, respectively, the maximum entrainment ratio achievable was 1.282. Furthermore, the efficiency of an ejector from Ariafar's work [31], under the same boundary conditions, was reported to be 0.9 using CFD simulation. This established the limit of the attainable entrainment ratio and highlighted the need to modify the ejector's geometry based on a described 1D iterative model to achieve the maximum entrainment ratio. The flowchart in the Fig. 4 outlines the approach taken. It is noteworthy that the optimization process for determining the optimal dimension, such as the ejector throat diameter in our case, can also be achieved through optimization algorithms. One widely utilized method is the genetic algorithm, which has been employed in various studies for diverse purposes, as documented in the literature [32], [33]. However, in our study, we utilize a 1D iterative model to compute the optimal ejector throat diameter to attain the maximum entrainment ratio. This 1D iterative model offers simplicity and directness, obviating the need for complex CFD simulations involving multiple parameters and conditions, as well as eliminating the necessity for optimization algorithms such as genetic algorithms or similar methods.

To approach the maximum entrainment ratio of 1.282, the area of the constant section was calculated to be 150 mm. This is compared to the diameter of 140 mm in Ariafar's ejector [31], with other dimensions also altered to maximize the entrainment ratio.

4.1 Designed operating conditions and dimensions

In Ariafar's study [31], flow simulation within a thermo-compressor was performed using computational fluid dynamics. To facilitate comparison with the current work, the boundary conditions listed in Table 1 were preserved unchanged. The mesh utilized consisted of approximately 420,000 quadrilateral cells. Varying the mesh size revealed that the solution was dependent on the cell number.

The primary and suction steam boundary conditions were defined as "pressure inlet," while the discharge steam boundary condition was defined as pressure outlet. The pressure and temperature values at these boundaries are provided in
Table **1**.

Numerous geometries and dimensions were employed to maximize the entrainment ratio, with the diameter of the ejector throat set at 150 mm as calculated from the previously described 1D iterative model. Other dimensions can be seen in Fig. 5. While the ejector's throat diameter remained unchanged in all simulations, the mixing chamber angle, nozzle x position (NXP), and some other dimensions were varied to investigate the extent to which CFD results could approach the entrainment ratio limit established by the 1D iterative model in the previous section.

Table 1. Designed operating conditions of the ejector.

Boundary	Pressure (kPa)	Temperature (^{0}C)
Primary steam	700	165
Secondary steam	22.87	63
Discharge	40	73

Dimensions of the final geometry which led to the maximum entrainment ratio are shown in the following image:

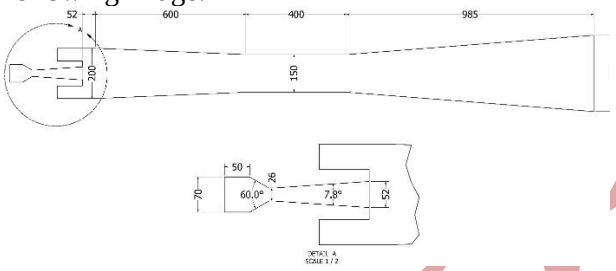

Fig. 5. Dimensions of the final geometry of the ejector.

4.2 Ejector numerical model

In our simulation of gas ejectors, a 2D axisymmetric numerical model is employed, and this choice is justified based on both practical considerations and computational efficiency. Gas ejectors typically exhibit axial symmetry, allowing us to exploit the symmetry of the geometry to reduce the computational domain without compromising the accuracy of the results significantly. The 2D axisymmetric model results in a satisfactory level of accuracy for both overall and localized flow phenomena [34]. This approach aligns with findings in the literature, indicating that a 2D axisymmetric model offers comparable results to a 3D flow model while requiring less computational effort [15]. Utilizing axisymmetric conditions, the study solves the 2D governing equations, expressed in terms of radial components, through a finite volume discretization method with a second-order upwind scheme [35].

4.3 Governing equations for ejector numerical model

The numerical simulation of the gas ejector involves solving the compressible Navier-Stokes equations for conservation of mass, momentum, and energy. In axisymmetric coordinates (r, θ, z), the governing equations for the compressible flow in a 2D axisymmetric model are:

1.Continuity Equation

$$\frac{\partial(\rho r)}{\partial t}+\frac{1}{r}\frac{\partial}{\partial r}(\rho r u_r)+\frac{\partial(\rho u_z)}{\partial z}=0 \quad (20)$$

2.Radial Momentum Equation:

$$\frac{\partial(\rho u_r)}{\partial t}+\frac{1}{r}\frac{\partial}{\partial r}(\rho u_r^2)+\frac{\partial(\rho u_r u_z)}{\partial z}=-\frac{\partial p}{\partial r}+\frac{\mu}{r}\frac{\partial}{\partial r}\left(r\frac{\partial u_r}{\partial r}\right)+\frac{\mu}{r^2}\frac{\partial^2 u_r}{\partial \theta^2} \quad (21)$$

3.Axial Momentum Equation:

$$\frac{\partial(\rho u_z)}{\partial t}+\frac{1}{r}\frac{\partial}{\partial r}(\rho u_r u_z)+\frac{\partial(\rho u_z^2)}{\partial z}=-\frac{\partial p}{\partial z}+\frac{\mu}{r}\frac{\partial}{\partial r}\left(r\frac{\partial u_z}{\partial r}\right)+\frac{\mu}{r^2}\frac{\partial^2 u_z}{\partial \theta^2} \quad (22)$$

3.Energy Equation*:*

$$\frac{\partial(\rho E)}{\partial t}+\frac{1}{r}\frac{\partial}{\partial r}\left[\rho u_r\left(H+\frac{u_r^2}{2}\right)\right]+\frac{\partial}{\partial z}\left[\rho u_z\left(H+\frac{u_z^2}{2}\right)\right]=\frac{\partial}{\partial r}\left(\frac{k}{\mu}\frac{\partial T}{\partial r}\right)+\frac{\partial}{\partial z}\left(\frac{k}{\mu}\frac{\partial T}{\partial z}\right) \quad (23)$$

4.4 Numerical solution in ANSYS Fluent

The aforementioned governing equations are discretized and solved numerically using ANSYS Fluent software. The software employs finite volume method to discretize the governing equations, and the resulting system of algebraic

equations is solved iteratively until convergence is achieved. Appropriate boundary conditions, turbulence models (SST k-ω), and solver settings are specified in ANSYS Fluent to accurately capture the flow physics within the gas ejector system. The use of a 2D axisymmetric model combined with the numerical capabilities of ANSYS Fluent allows for a computationally efficient yet accurate simulation of gas ejector performance. The selected solver configuration adopts a Density-Based Solver (DBS), which is particularly well-suited for simulations involving significant density variations, as commonly encountered in compressible flow regimes. Additionally, a Second Order Method has been implemented for the spatial discretization scheme.

4.5 Turbulence model selection

In the context of CFD simulation for gas ejectors, the choice of an appropriate turbulence model is crucial for accurate predictions. To assess CFD accuracy, the relative error is computed between numerical and experimental entrainment ratios [36]. For this study, the k-ω SST turbulence model is chosen based on the insights provided by Bartosiewicz et al. [37], who highlighted its superior performance in predicting shock waves phase, strength, and mean line of pressure recovery. In alignment with Hemidi et al.'s [36] observations, which suggest that while k-ε Standard may excel globally, k-ω SST and k-ε Standard may yield similar results in global quantities but differ in local flow characteristics. The literature review further endorses the appropriateness of k-ω SST for gas ejector simulations, with multiple studies ([3], [36] and [37]) affirming its effectiveness in predicting shock wave, stream mixing, and critical conditions. The chosen turbulence model significantly influences the accuracy of simulations, and the extensive comparison of turbulence models presented in the literature positions k-ω SST as a robust and reliable choice for this study ([3] and [37]).

4.6 Working fluids properties

The density of the working fluids was determined utilizing the ideal gas equation, a methodology commonly employed in various references [38]–[43] . In contrast, specific heat, thermal conductivity, and viscosity were deduced from the authentic thermodynamic properties of the respective working fluids, specifically water vapor, based on the IAPWS-IF97 formulation.

4.7 Spatial discretization approach

The prevailing belief in the field suggests that as long as a spatial discretization scheme maintains second-order accuracy, it effectively mitigates false diffusion. Employing a sufficiently fine mesh is known to yield accurate results even with a lower-order scheme, while a higher-order discretization scheme comes at the cost of increased computational resources. In the simulation of a steam ejector, the emphasis was primarily on utilizing the second-order upwind scheme, with limited consideration given to the potential impact of the spatial discretization scheme and mesh density [44].
The selected discretization schemes included the widely employed second-order upwind scheme. For addressing the pressure equation, the PRESTO scheme, specifically designed for flows featuring steep pressure gradients, was chosen.

4.8 Convergence criteria

The convergence is considered achieved when the following conditions are met:

- The residual terms reach values lower than 10^{-5} and exhibit stability throughout the simulation.
- The calculated mass flows at each face remain stable, and the disparity in mass flow between the two inlet flows and the outlet flow of the ejector is less than 10^{-7} kg/s.
- The maximum velocity value at the inlet of the ejector throat attains stability.

4.9 CFD model validation

4.9.1 Validation Approach:

The validation of our CFD approach involves an examination of the ejector's performance under various conditions. Given the unique dimensions and boundary conditions of our ejector, direct validation becomes a challenge. To ensure the credibility of our approach, we adopted a multi-faceted validation strategy.

In the case of Al-Doori's work [10], our validation concentrated on the static pressure distribution along the ejector. This detailed analysis allowed us to compare our CFD results with Al-Doori's experimental data, providing a robust validation of our approach against a known ejector configuration.

Simultaneously, for Ariafar's study [31], we focused on validating the performance curve of the ejector. By comparing our CFD results with Ariafar's findings for specific primary and suction steam pressure and temperature at various back pressures, we verified the accuracy of our approach in capturing the intricacies of ejector performance under different operating conditions.

4.9.2 Validation against Al_Doori's experiments:

To validate our CFD approach, we compared our simulations with experiments conducted by Al_Doori [10], focusing on the examination of static pressure distribution along the ejector. The primary stream conditions considered for this validation were a pressure of 270 kPa, a temperature of 130 °C, with an evaporator operating at 10°C, and a condenser pressure of 6 kPa. The work by Al-Doori [10] provides information on the geometry and dimensions of this ejector.

4.9.2.1 Mesh independence analysis:

In order to ascertain the mesh independence of our computational simulations, a systematic grid convergence study was conducted for the work of Al-Doori [10]. Various mesh densities were explored, and the resulting entrainment ratios were analyzed to determine the convergence trends. The outcomes are depicted in Fig. 6 and Table 2.

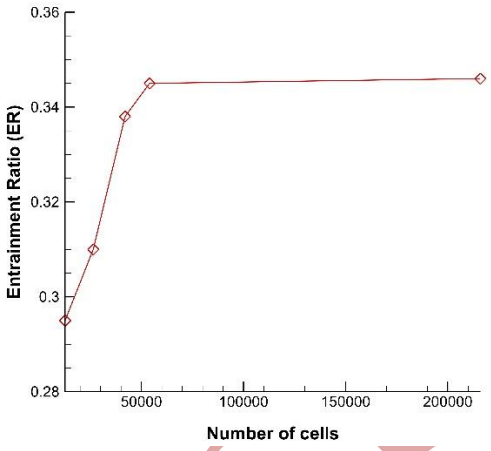

Fig. 6. Grid independence study: entrainment ratio variation in an ejector across different mesh densities of Al-Doori's work [10].

Table 2. Mesh independence study for entrainment ratio.

Mesh number	Number of cells	Entrainment Ratio (ER)
Mesh 1	12,600	0.295
Mesh 2	26,400	0.310
Mesh 3	42,000	0.338
Mesh 4	54,000	0.345
Mesh 5	216,000	0.346

Upon careful examination of the results, it is observed that the entrainment ratio exhibits a consistent trend of convergence as the mesh density increases. Notably, the entrainment ratio experiences little change between Mesh 4 and Mesh 5, indicating a stabilization of results with mesh refinement.

After a thorough analysis of convergence trends, solution stability, and key flow metrics, it is concluded that Mesh 4 provides a reliable and converged representation of the entrainment

ratio. The minimal change in entrainment ratio between Mesh 4 and Mesh 5 suggests that the results have achieved mesh independence at the selected density.

This determination is further supported by the absence of significant oscillations or irregular behavior in the convergence trends. Consequently, Mesh 4 is deemed adequate for our simulations, and the entrainment ratio is considered to be mesh-independent at this resolution.

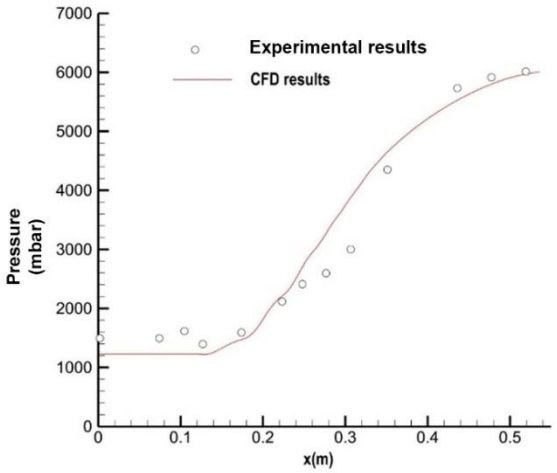

Fig. 7. Comparison of CFD and experimental results for static pressure along the ejector, based on Al_Doori's work [10]. primary stream conditions: 270 kPa, 130 °C, with an evaporator temperature of 10°C, and a condenser pressure of 6 kPa.

Our CFD results for both entrainment ratios and static pressure along the ejector are in close concordance with the ecperimental results reported by Al-Doori et al. [10] as seen in Fig. 7.

4.9.2.2 Validation against Ariafar's study:

As a reference for our study, we initially validated the entrainment ratio versus pressure (performance curve) using Ariafar's study [31]. Ariafar's ejector, with a throat diameter of 140 mm, served as the baseline for our comparison. The boundary conditions for both Ariafar's original geometry and our optimized geometry (throat diameter of 150 mm) were set as follows:

- Primary Steam: Pressure 700 kPa, Temperature 165 °C
- Secondary Steam: Pressure 22.87 kPa, Temperature 63 °C
- Discharge: Pressure 30-65 kPa

Our aim was to replicate Ariafar's reported entrainment ratio of 0.9 under these conditions. Subsequently, we applied the same approach to our ejector, with modifications in throat diameter and other parameters based on our 1D model optimization.

4.9.2.3 Mesh independence analysis for Ariafar's study:

To ensure the accuracy and reliability of our computational simulations, a comprehensive mesh independence study was conducted for the ejector geometry as reported by Ariafar [31]. The mesh densities were systematically varied, and the resulting entrainment ratios (ER) were examined to ascertain convergence trends. Table 3 and Fig. 8 illustrate the mesh dependency test conducted for this ejector, demonstrating its entrainment ratio across different mesh densities.

Table 3. Mesh independence study for entrainment ratio.

Mesh number	Number of cells	Entrainment Ratio (ER)
Mesh 1	102,000	0.842
Mesh 2	159,375	0.863
Mesh 3	386,400	0.917
Mesh 4	420,000	0.930
Mesh 5	680,000	0.931

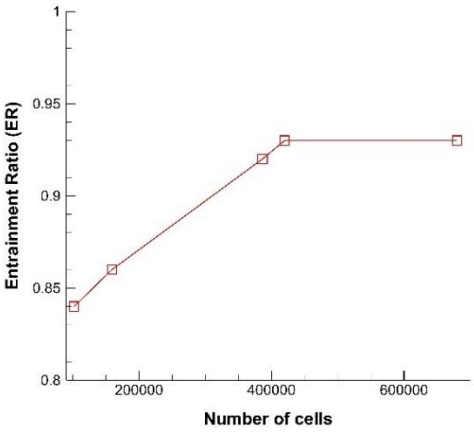

Fig. 8. Comparison of CFD and experimental results for static.

Analysis of the results reveals a consistent trend of convergence in the entrainment ratio as the mesh density increases. Particularly, Mesh 4 demonstrates a stabilized entrainment ratio, indicating mesh independence. This observation is further supported by the minimal change in entrainment ratio between Mesh 4 and Mesh 5.
For both the original ejector geometry (throat diameter of 140 mm, as in Ariafar's work) and our modified geometry (throat diameter of 150 mm), Mesh 4 was selected as the optimal mesh density. The entrainment ratios obtained at this mesh density remain virtually unchanged between the two geometries, suggesting that the results are not only mesh-independent but also robust across different ejector configurations.

This careful consideration of mesh independence ensures the reliability of our simulations and provides a solid foundation for subsequent analyses, discussions, and comparisons.

4.9.2.4 CFD results for validation of Ariafar's study:

In this sub-chapter, we present the CFD results obtained during the validation of Ariafar's study, focusing on the entrainment ratio versus back pressure. The primary stream conditions considered for this validation were set at Primary Steam: Pressure 700 kPa, Temperature 165 °C, and Secondary Steam: Pressure 22.87 kPa, Temperature 63 °C.
The entrainment ratio results are depicted in Fig. 9, illustrating the relationship between entrainment ratio and back pressure. Notably, the entrainment ratio is a crucial performance parameter that directly influences the ejector's efficiency.
The CFD results of our study, where we systematically re-simulated Ariafar's work for the ejector with a throat diameter of 140 mm, exhibit a remarkable agreement with Ariafar's original CFD results. The concordance between the two sets of results is evident across various back pressures, reaffirming the robustness and accuracy of our CFD approach in replicating the performance of the ejector under the specified conditions.

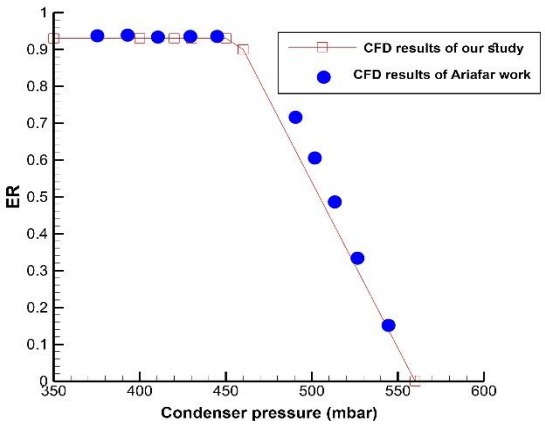

Fig. 9. Ejector performance curve - a comparative analysis between CFD results from this study and Ariafar's investigation [31].

This close alignment between our CFD results and those of Ariafar for the throat diameter of 140 mm serves as a crucial validation step. It instills confidence in the reliability of our CFD methodology and sets a solid foundation for the subsequent analysis in the following section. The upcoming section will focus on the modified geometry, featuring a throat diameter of 150 mm, and this validation provides assurance that our results for the modified geometry are built upon a validated and trustworthy CFD framework.

4.2 CFD results

Fig. 10 depicts the Mach number contours for the altered ejector, featuring a throat diameter of 150 mm, under the conditions of Primary Steam: Pressure 700 kPa, Temperature 165 °C, and Secondary Steam: Pressure 22.87 kPa, Temperature 63 °C.

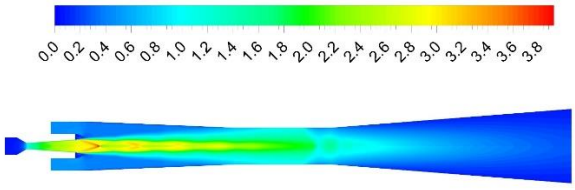

Fig. 10. Contours of Mach number.

The entrainment ratio for this ejector is calculated by CFD method 1.25 while the maximum theoretical value calculated by the 1D

model is 1.282 so the efficiency of this optimized geometry is:

$$\eta_{_2} = \frac{1.25}{1.282} = 97.7\%$$

This value holds significant importance as it signifies that the entrainment ratio of the ejector is nearing its optimal value and cannot be substantially enhanced by modifying the ejector's dimensions and geometry. Furthermore, this validates the optimal throat diameter obtained through the 1D model. Employing this innovative method, the entrainment ratio of a literature-based ejector was enhanced from 0.9 to 1.25 while maintaining the same boundary conditions, which translates to a notable improvement of approximately 39%. This improvement implies a 39% reduction in the consumption of live steam necessary to compress the same quantity of suction steam.

5. Conclusions

The present investigation introduces new ejector efficiency definitions based on a 1D model. The second definition, which relates the entrainment ratio of a designed ejector under specific boundary conditions to that of an ideally designed ejector, represents a novel and valuable parameter. It quantifies the degree of an ejector's departure from its ideal design and its potential for entrainment ratio improvement.

To assess the accuracy of the proposed 1D model, the ejector dimensions were recalculated for a specified boundary condition based on relevant literature. The entrainment ratio of the selected ejector in the literature was determined to be 0.7, while the 1D model predicted that an entrainment ratio of up to 1.282 could be theoretically achieved under the same boundary conditions, with further enhancement being theoretically impossible. To explore the limiting entrainment ratio, numerous geometries and dimensions were examined using commercial computational fluid dynamics (CFD) software, namely Ansys Fluent.

The computational fluid dynamics (CFD) results yielded a maximum entrainment ratio of 1.25, which is pretty close to the theoretical maximum value. This example serves to demonstrate the potential for improving the efficiency of an ejector and the extent to which such improvements may be achieved. In summary, the present study introduced three efficiency measures that may be useful in various contexts:

Efficiency #1 enables the comparison of a steam ejector with a system comprising a steam turbine, compressor, and mixer.

Efficiency #2 may be utilized to determine the extent to which the entrainment ratio of an ejector may be enhanced under given boundary conditions, by modifying the geometry and dimensions of the ejector to increase its efficiency.

Efficiency measure #3 pertains to an ejector in which the main dimensions (i.e., throat diameter of the ejector and primary nozzle) are fixed, and compares the entrainment ratio of the ejector to an ideal ejector with the same primary nozzle and ejector throat diameters, in which no irreversibilities or losses occur.

It should be noted that the proposed one-dimensional (1D) model is subject to several simplifying assumptions, such as the use of a single-phase, non-condensing gas, adiabatic processes, isentropic expansion, and so forth. Although it is possible for numerical or experimental results to exceed the calculated limiting entrainment ratio for a specific design, this value remains a valuable tool for evaluating and designing ejectors.

For future studies, it is recommended to compare the entrainment ratio obtained via experimental or numerical techniques with the 1D efficiency measure proposed in this work. It is also suggested that future numerical simulations employ a wet steam model, as steam condensation may enhance mixing and increase the entrainment ratio.

References

[1] J. Chen, S. Jarall, H. Havtun, and B. Palm, “A review on versatile ejector applications in refrigeration systems”, *Renew. Sust. Energ. Rev.*, Vol. 49, pp. 67–90, (2015).

[2] V. V. Chandra and M. R. Ahmed, "Experimental and computational studies on a steam jet refrigeration system with constant area and variable area ejectors", *Energy Convers. Manag.*, Vol. 79, pp. 377–386, (2014).

[3] N. Ruangtrakoon, T. Thongtip, S. Aphornratana, and T. Sriveerakul, "CFD simulation on the effect of primary nozzle geometries for a steam ejector in refrigeration cycle", *Int. J. Therm. Sci.*, Vol. 63, pp. 133–145, (2013)

[4] F. Liu, E. A. Groll, and D. Li, "Investigation on performance of variable geometry ejectors for CO 2 refrigeration cycles", *Energy.*, Vol. 45, No.1, pp.829–839 ,(2012).

[5] A. Milazzo, A. Rocchetti, and I. W. Eames, "Theoretical and Experimental Activity on Ejector Refrigeration", *Energy Procedia*, Vol. 45, pp. 1245–1254, (2014).

[6] J. M. Abdulateef, K. Sopian, M. A. Alghoul, and M. Y. Sulaiman, "Review on solar-driven ejector refrigeration technologies", *Renewable and Sustainable Energy Reviews*, Vol. 13, No. 6–7, pp. 1338–1349, (2009).

[7] V. M. Nguyen, S. B. Riffat, and P. S. Doherty, "Development of a solar-powered passive ejector cooling system", *Appl. Therm. Eng.*, Vol. 21, No. 2, pp. 157–168, (2001).

[8] M. Alperin and J.-J. Wu, "Thrust Augmenting Ejectors, Part I", *AIAA Journal*, Vol. 21, No. 10, pp. 1428–1436, (1983).

[9] P. Sreekireddy, T. K. K. Reddy, V. Dadi, and P. Bhramara, "CFD Simulation of Steam Ejector System in High Altitude Test (HAT) Facility", in *ASME 2012 Gas Turbine India Conference*, American Society of Mechanical Engineers, pp. 149–157, (2013)

[10] G. F. L. Al-Doori, "Investigation of refrigeration system steam ejector performance through experiments and computational simulations", PhD Thesis, University of Southern Queensland, (2013).

[11] S. Varga, A. C. Oliveira, and B. Diaconu, "Influence of geometrical factors on steam ejector performance – A numerical assessment", *Int. J. Refrig.*, Vol. 32, No. 7, pp. 1694–1701, (2009).

[12] N. Sharifi and M. Sharifi, "Reducing energy consumption of a steam ejector through experimental optimization of the nozzle geometry", *Energy*, Vol. 66, pp. 860–867, (2014).

[13] N. Sharifi and M. Sharifi, "Experimental Improvement of Ejector Performance Through Numerical Optimization of Nozzle Geometry", ASME, San Diego, pp. 1–9, (2013).

[14] S. Varga, A. C. Oliveira, and B. Diaconu, "Numerical assessment of steam ejector efficiencies using CFD", *Int. J. Refrig.*, Vol. 32, No. 6, pp. 1203–1211, (2009).

[15] K. Pianthong, W. Seehanam, M. Behnia, T. Sriveerakul, and S. Aphornratana, "Investigation and improvement of ejector refrigeration system using computational fluid dynamics technique". *Energy Convers. Manag.*, Vol. 48, No. 9, pp. 2556–2564, (2007).

[16] A. Mohammadi, "An investigation of geometrical factors of multi-stage steam ejectors for air suction", *Energy*, Vol. 186, p. 115808, (2019).

[17] L. Wang, J. Liu, T. Zou, J. Du, and F. Jia, "Auto-tuning ejector for refrigeration system", *Energy*, Vol. 161, pp. 536–543, (2018).

[18] I. W. Eames, A. E. Ablwaifa, and V. Petrenko, "Results of an experimental study of an advanced jet-pump refrigerator operating with R245fa", *Appl. Therm. Eng.*, Vol. 27, No. 17–18, pp. 2833–2840, (2007).

[19] A. J. Meyer, T. M. Harms, and R. T. Dobson, "Steam jet ejector cooling powered by waste or solar heat", *Renew. Energy*, Vol. 34, No. 1, pp. 297–306, (2009).

[20] Y. Zhu, W. Cai, C. Wen, and Y. Li, "Numerical investigation of geometry parameters for design of high performance ejectors", *Appl. Therm. Eng.*, Vol. 29, No. 5–6, pp. 898–905, (2009).

[21] P. Pei *et al.*, "Numerical studies on wide-operating-range ejector based on anodic pressure drop characteristics in proton exchange membrane fuel cell system", *Appl. Energy*, Vol. 235, pp. 729–738, (2019)

[22] C. Li, Y. Li, W. Cai, Y. Hu, H. Chen, and J. Yan, "Analysis on performance characteristics of ejector with variable area-ratio for multi-evaporator refrigeration system based on experimental data", *Appl. Therm. Eng.*, Vol. 68, No. 1–2, pp. 125–132, (2014).

[23] S. Varga, P. M. S. Lebre, and A. C. Oliveira, "CFD study of a variable area ratio ejector using R600a and R152a refrigerants", *Int. J. Refrig.*, Vol. 36, No. 1, pp. 157–165, (2013).

[24] M. Dennis and K. Garzoli, "Use of variable geometry ejector with cold store to achieve high solar fraction for solar cooling", *Int. J. Refrig.*, Vol. 34, No. 7, pp. 1626–1632, (2011).

[25] A. Hakkaki-Fard, Z. Aidoun, and M. Ouzzane, "A computational methodology for ejector design and performance maximisation", *Energy Convers. Manag.*, Vol. 105, pp. 1291–1302, (2015).

[26] R. Yapıcı, H. K. Ersoy, A. Aktoprakoğlu, H. S. Halkacı, and O. Yiğit, "Experimental determination of the optimum performance of ejector refrigeration system depending on ejector area ratio", *Int. J. Refrig.*, Vol. 31, No. 7, pp. 1183–1189, (2008).

[27] Y. Jia and C. Wenjian, "Area ratio effects to the performance of air-cooled ejector refrigeration cycle with R134a refrigerant", *Energy Convers. Manag.*, Vol. 53, No. 1, pp. 240–246, (2012).

[28] T. Utomo, M. Ji, P. Kim, H. Jeong, and H. Chung, "CFD analysis of influence of converging duct angle on the steam ejector performance", *Int. Conf. Eng. Opt. EngOpt*, (2008).

[29] K. Banasiak *et al.*, "A CFD-based investigation of the energy performance of two-phase R744 ejectors to recover the expansion work in refrigeration systems: An irreversibility analysis", *Int. J. Refrig.*, Vol. 40, pp. 328–337, (2014).

[30] S. Elbel and P. Hrnjak, "Experimental validation of a prototype ejector designed to reduce throttling losses encountered in transcritical R744 system operation", *Int. J. Refrig.*, Vol. 31, No. 3, pp. 411–422, (2008).

[31] K. Ariafar, "Performance evaluation of a model thermocompressor using computational fluid dynamics," *Int. J. Mech.*, Vol. 6, No. 1, pp. 35–42, (2012).

[32] S. Acharya, V. K. Mishra, S. Chaudhuri, J. K. Patel, P. Ghose, and V. R. Kar, "Decision Support System for Porous Ceramic Matrix-based Burner by Hybrid Genetic Algorithm-Supervised Kohonen Map: A Comparative Assessment of

Performance of Neural Network Under Different Minor Attributes", *Arab J. Sci. Eng.*, Vol. 49, No. 2, (2024),

[33] M. M. A. Ansari, K. B. Sahu, S. Chaudhuri, J. Srikanth, D. Sahu, and V. K. Mishra, "Hybrid genetic algorithm-self organizing map network for decision support system: An application in combined mode conduction-radiation heat transfer in porous medium", *Numer. Heat Transf.*, Vol. 84, No. 5, pp. 642-664 , (2023).

[34] J. A. Expósito Carrillo, F. J. Sánchez de La Flor, and J. M. Salmerón Lissén, "Single-phase ejector geometry optimisation by means of a multi-objective evolutionary algorithm and a surrogate CFD model", *Energy*, Vol. 164, pp. 46–64, (2018)

[35] F. Riaz, P. S. Lee, and S. K. Chou, "Thermal modelling and optimization of low-grade waste heat driven ejector refrigeration system incorporating a direct ejector model", *Appl. Therm. Eng.*, Vol. 167, p. 114710, (2020)

[36] A. Hemidi, F. Henry, S. Leclaire, J. M. Seynhaeve, and Y. Bartosiewicz, "CFD analysis of a supersonic air ejector. Part I: Experimental validation of single-phase and two-phase operation", *Appl. Therm. Eng.*, Vol. 29, No. 8–9, pp. 1523–1531, (2009).

[37] Y. Bartosiewicz, Z. Aidoun, P. Desevaux, and Y. Mercadier, "Numerical and experimental investigations on supersonic ejectors", *Int. J. Heat Fluid Flow*, Vol. 26, No. 1, pp. 56–70, (2005)

[38] T. Sriveerakul, S. Aphornratana, and K. Chunnanond, "Performance prediction of steam ejector using computational fluid dynamics: Part 1. Validation of the CFD results", *Int. J. Therm. Sci.*, Vol. 46, No. 8, pp. 812–822, (2007).

[39] Y. Zhu and P. Jiang, "Experimental and numerical investigation of the effect of shock wave characteristics on the ejector performance", *Int. J. Refrig.*, Vol. 40, pp. 31–42, (2014).

[40] M. J. Opgenorth, D. Sederstrom, W. McDermott, and C. S. Lengsfeld, "Maximizing pressure recovery using lobed nozzles in a supersonic ejector", *Appl. Therm. Eng.*, Vol. 37, pp. 396–402, (2012).

[41] H. Wu, Z. Liu, B. Han, and Y. Li, "Numerical investigation of the influences of mixing chamber geometries on steam ejector performance", *Desalination*, Vol. 353, pp. 15–20, (2014).

[42] J. Dong, M. Yu, W. Wang, H. Song, C. Li, and X. Pan, "Experimental investigation on low-temperature thermal energy driven steam ejector refrigeration system for cooling application", *Appl. Therm. Eng.*, Vol. 123, pp. 167–176, (2017).

[43] Y. Wu, H. Zhao, C. Zhang, L. Wang, and J. Han, "Optimization analysis of structure parameters of steam ejector based on CFD and orthogonal test", *Energy*, Vol. 151, pp. 79–93, (2018).

[44] J. Xiao *et al.*, "Assessment of Different CFD Modeling and Solving Approaches for a Supersonic Steam Ejector Simulation", *Atmosphere*, Vol. 13, No. 1, pp. 1–26, (2022).